IEEE Access
Multidisciplinary | Rapid Review | Open Access Journal

Received February 6, 2020, accepted March 9, 2020, date of publication March 19, 2020, date of current version April 8, 2020.

Digital Object Identifier 10.1109/ACCESS.2020.2981961

A Design Method of Air-Cooled Radiator Based on Electric Aircraft Controller

SHULI WANG[1,2], XING CUI[3], SHAOHUA MA[1], ZHEYUAN PANG[1], YUNING FENG[1], AND SHUO ZHANG[4]

[1]School of Electrical Engineering, Shenyang University of Technology, Shenyang 110023, China
[2]Key Laboratory of General Aviation, Shenyang Aerospace University, Shenyang 110136, China
[3]China North Vehicle Research Institute, Beijing 100072, China
[4]National Engineering Laboratory for Electric Vehicles, School of Mechanical Engineering, Beijing Institute of Technology, Beijing 100081, China

Corresponding author: Shaohua Ma (mash_dq@sut.edu.cn)

This work was supported in part by the Foundation Department of Education Liaoning Province under the Project Name: Study on energy efficiency optimization of electric propulsion system (Grant LZGD2017041), in part by the Foundation of Research and Development Plan in key Areas of Guangdong Province under the Project Name: Integration and industrialization of high performance, long endurance and integrated electric drive system (Grant 2019B090910001), and in part by the National Nature Science Foundation of China under the Project Name: Research on motor optimization design of electric aircraft main drive based on multi-physical field coupling (Grant 51607115).

ABSTRACT The air-cooled motor controller has been widely used in electric aircraft due to its simple heat dissipation structure and maintenance-free features. Being the main heating component of the electric propulsion system of electric aircraft, the weight and the volume of the air-cooled motor controller need to be strictly controlled. Due to the short power running time of the electric motor controller, there is a large weight and volume allowance margin for the air-cooled radiatorbased on the rated power and heat dissipation requirements of the motor controller.This paper proposes an air-cooled radiator design method that can reduce its volume and weight by optimizing its structure based on the operating conditions of the electric aircraft under the heat dissipation requirements.The structure of the air-cooled motor can be optimized by optimizing the structure the minimum structure of the motor controller radiator constrained by the maximum temperature of the Insulated Gate Bipolar Transistor (IGBT) module,which can be determined using an algorithm called the motor controller thermal resistance network model. Experimental results obtained from a prototype test on a two-seat electric aircraft demonstrate the effectiveness of the optimization method. The air-cooled radiator designed using the proposed method can be reduced by 5% in weight while meeting the heat dissipation requirements of the motor controller of the electric aircraft.

INDEX TERMS Electric aircraft, motor controller, IGBT module, air-cooled radiator, thermal resistance network model.

I. INTRODUCTION

With environmental pollution getting increasingly serious, the concept of ''Lucid waters and lush mountains are invaluable assets'' has been gradually recognized by the public. As a new energy vehicle, electric aircraft has been widely favored for its zero emission, no pollution, low noise, simple structure, good ride comfort and many other advantages [1]. Motor controller is the core component of electric aircraft and one of the main heating elements of electric aircraft with IGBT module being the main heating source of motor controller. Due to the high integration of IGBT module, the heat flux density per unit volume can be very large and can be easily damaged under poor cooling conditions and large currents, which may lead to severe damage to reliability of the motor controller [2]. The radiator of motor controller mainly consists of air-cooled and water-cooling structures. Water cooling structure are small in size and strong in heat dissipation capacity, while it has complex auxiliary structure and low reliability as it needs to be equipped with auxiliary equipment such as water pump, water tank, heat exchanger and pipeline [3]. On the other hand, air-cooled heat dissipation structure is simple in structure, highly reliable, and has no requirement for auxiliary equipment. However, its heat dissipation capability is poor, and the size and weight of the radiator are larger than other under the same power level [4]. Given the characteristics of electric aircrafts and battery energy density, reducing the take-off weight of the aircraft is an effective way to increase the lifespan of the aircraft [5]. Therefore, the air-cooled radiator structure is

The associate editor coordinating the review of this manuscript and approving it for publication was Jenny Mahoney.

more suitable for the electric aircraft motor controller because of its high reliability and light weight.

In order to meet the heat dissipation requirements of the motor controller under high current conditions, motor controllers are generally designed according to their rated power consumption in the design process of conventional air-cooled radiator of motor controller [6]. However, the actual flight profile is not taken into consideration. Flight profile of electric aircraft mainly contains three phases: take-off phase, cruise phase and landing phase. Aircraft requires motor controller to operate at rated power only during the take-off phase which lasts for a short period of time. During the cruise phase, the power requirement of the motor controller is only about 1/3 of the rated power. While in the landing phase; the power requirement is even less [7]. Obviously, the design of the radiator according to the heat dissipation requirement of the conventional motor controller at the rated power yields a larger design margin, and consequently the designed radiator has a large weight and volume [8].This paper proposed an optimal design method for the radiator structure based on the operating conditions of the electric aircraft, which can reduce size and weight of the radiator.The heat dissipation of the motor controller is optimized according to the flight profile of electric aircraft while ensuring that the IGBT module does not over-heat during operation. By reducing the size and the weight of the controller radiator, the weight of the electric propulsion system of electric aircraft can be reduced, which can significantly improve the lifespan of the electric aircraft [9].

IGBT module is the main heating device of the aircraft motor controller.The optimization of air-cooled radiator for motor controller mainly contains two methods, which are finite element analysis and thermal resistance network [10]. The finite element analysis method establishes a heat conduction model and meshes it. Once the boundary condition is determined, the temperature field distribution of the heat conduction model can be obtained by solving the differential equation [11].This method can truly reflect the distribution of the internal temperature field of the motor controller, albeit relying on a large amount of accurate support sample data. However, heat of the IGBT module is mainly transmitted to the air-cooled radiator through multiple layers of different martial, whose thermal conductivity is hard to estimate, large calculation error and even unreasonable design optimization still happens [12]. On the other hand, the thermal resistance network method is a method based on the equivalent thermal resistance to the heat loss during the process of transferring the heat generated by the IGBT chip to each physical layer [13]. The thermal resistance network method is an empirical method; it can quickly calculate the loss of each physical layer, which is convenient for real-time simulation. However, the thermal resistance network method can only estimate the mean temperature of each physical layer and cannot reflect the temperature distribution of each physical layer [14]. In addition, some parameters possibly affecting temperature are ignored when establishing the thermal resistance network model, which could make the thermal resistance network model incapable of reflecting the real-time heat transfer and heat dissipation inside the motor controller [15]. Given the fact that electric aircraft motor controller requires no real-time monitoring of internal temperature dissipation but ensuring internal temperature being in the allowed range, the thermal resistance network method is more suitable for the optimal design of the motor controller air-cooled radiator [16].

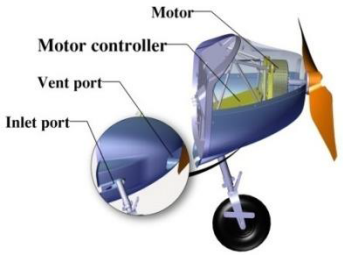

FIGURE 1. Schematic diagram of the internal structure of a two-seat electric aircraft engine compartment.

This paper proposes a motor controller air-cooler design optimization method. For more accurate analysis, we firstly design an air-cooler based on conventional motor controller cooler for a two-seat aircraft and build a thermal resistance network model using heat loss data collected from actual flight operation and wind velocity simulated using a turbine system [17]. The structure of the air-cooler can then be optimized by determining the its minimum height under the maximum allowed temperature of the IGBT module, whose temperature under different operation conditions can be obtained by using the thermal resistance network model and system heat loss. The size and weight of the air-cooler can be consequently reduced [18]. Experimental results from prototype aircraft test suggest that the proposed method can provide very accurate air-cooler analysis, consequently, leads to more optimized design with less volume and weight. Compared to conventional design method, the propose method can reduce weight of air-cooler by 5%, which can further improve the propulsion system of electric aircraft.

II. COOLING SYSTEMS

As a core member of electric aircraft, electric aircraft motor controller is normally located at the nose of the plane of the aircraft engine room. Fig.1 shows the internal structure of the engine compartment of a two-seat electric aircraft. The motor controller is placed at the rear of the motor. In order to meet the heat dissipation requirements of the motor controller, air outlet holes are opened in the front and rear portions of the engine compartment fairing [19], respectively. During the operation of the aircraft, the airflow enters from the front in take opening of the aircraft engine compartment fairing, and exits from the rear air outlet.The flow-rateis approximately equal to the incoming flow speed of the aircraft during flight [20].

Being one of the main heating components of the electric aircraft, the motor controller contains many electronic

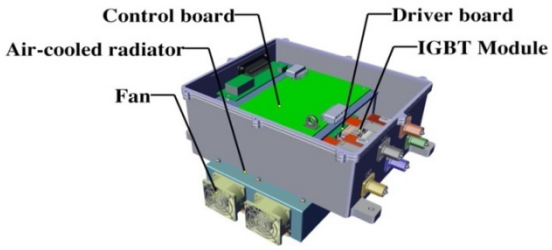

FIGURE 2. Schematic diagram of the motor controller.

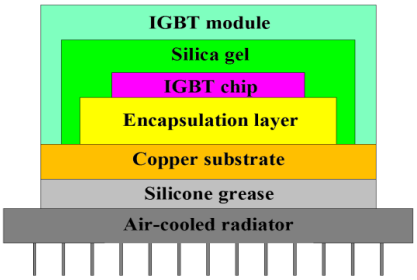

FIGURE 3. Schematic diagram of heat transfer from the motor controller.

components. From the structural point of view, the motor controller is mainly composed of a control board, a drive board, an IGBT module, an air-cooled radiator and a casing [21]. IGBT module is the main heat source of motor controller, which contributes most of the system loss of the motor controller. Therefore, system loss of other parts of motor controller is ignored. Fig. 2 shows a motor controller of the type aircraft described in this paper in which the control board is installed at the top of the controller and the driver board is installed on the IGBT module.The IGBT module substrate is fixed on the upper surface of the air-cooled radiator, which usually adopts the traditional heat dissipation structure [22]. Usually, in order to enhance the heat dissipation effect of the radiator, the outer surface of the IGBT module substrate is connected to the air-cooled radiator by thermal grease [23]. Fig. 3 shows a schematic diagram of the heat transfer of the motor controller. During the heat transfer process, the heat generated by IGBT module chip reaches the copper substrate through the IGBT module packaging layer, and eventually transfers to the air-cooled radiatorby radiating heat through heat convection with the outside environment. In order to simulate the actual flight profile, two adjustable speed fans are installed on the radiator fins to simulate the wind speed during the actual flight.

The system loss of the motor controller in the actual flight process is not only related to the flight conditions, but also related to the voltage and discharge current of the battery used in the electric aircraft. The system loss of the motor controller could be expressed as:

$$P_m(t) = V_{\mathrm{DC}}(t)I_{\mathrm{DC}}(t) - \sqrt{3}U_{\mathrm{rms}}(t)I_{\mathrm{rms}}(t)\cos\phi(t), \quad (1)$$

where t is the duration of take-off phase, $P_m(t)$ is the loss power of the motor controller; $V_{\mathrm{DC}}(t)$ is the output voltage of the battery during discharge, which is related to the discharge time of the battery; $I_{\mathrm{DC}}(t)$ is the output current of the battery during discharge; $U_{\mathrm{rms}}(t)$ is the output AC voltage of the controller; $I_{\mathrm{rms}}(t)$ is the output AC current of the controller; $\cos\phi(t)$ is the power factor.

Real time acquisition of input /output voltage, input / output current and power factor of motor controller, the input / output characteristic equation of controllercan be obtained via the interpolation method.

$$\begin{cases} V_{\mathrm{DC}}(t) = \sum_{i=0}^{4} a_i t^i \\ I_{\mathrm{DC}}(t) = \sum_{i=0}^{4} b_i t^i \\ U_{\mathrm{rms}}(t) = \sum_{i=0}^{4} c_i t^i \\ I_{\mathrm{rms}}(t) = \sum_{i=0}^{4} d_i t^i \\ \cos\phi(t) = \sum_{i=0}^{4} e_i t^i \end{cases} \quad (2)$$

The system loss of the motor controller in the actual flight process can be calculated according to Eqn. (1); In order to optimize the radiator design of motor controller, the system loss of motor controller should be calculated according to the actual operating conditions of the aircraft to initialize the thermal resistance model. The temperature of IGBT module can be later determined. The heat dissipation structure of the motor controller can then be optimized according to the actual operating conditions of the aircraft while allowing the highest IGBT module temperature.

III. CALCULATION OF TEMPERATURE OF IGBT MODULE

IGBT module is the main heat source of motor controller, whose malfunction is mainly caused by high temperature. It is necessary to ensure that the temperature of IGBT module is within the allowable working range to ensure reliable operation of the motor controller. Therefore, temperature calculation of IGBT module is particularly important. Under the premise of knowing the power consumption of the motor controller system, the thermal resistance network model could be built according to the heat balance theory to determine the temperature of the IGBT module.

IGBT module contains two main parts, IGBT and flywheel diode(FWD). Due to the short duration of the aircraft in the take-off phase, which is generally about 1∼3min. The heat dissipation system of IGBT module can be treated as a thermal behavior model under transient or short pulse current, which could be described by establishing a Partial Fraction Circuit model. The thermal impedance curve of the IGBT and FWD could be accurately expressed by the fourth-order Foster model, whose fitting coefficient is given in the IGBT module manual. Therefore, the fourth-order Foster model fitting could be performed according to the thermal impedance

curve of the IGBT and FWD to obtain the thermal impedance curve characteristic equation [24]:

$$\begin{cases} Z_{\mathrm{IGBT}}(t) = \sum_{i=1}^{4} R_i(1 - e^{-t/\tau}) \\ Z_{\mathrm{FWD}}(t) = \sum_{j=1}^{4} R_j(1 - e^{-t/\tau}), \end{cases} \tag{3}$$

where $Z_{\mathrm{IGBT}}(t)$ is the thermal impedance of the IGBT; $Z_{\mathrm{FWD}}(t)$ is the thermal impedance of the FWD; R_i is the thermal resistance fitting factor of the IGBT; R_j is the thermal resistance fitting coefficient of the FWD; τ is the IGBT and FWD Thermal time constant.

The thermal impedance of the IGBT and FWD is output in parallel and could be expressed as:

$$Z_{\mathrm{arm}}(t) = \frac{Z_{\mathrm{FWD}}(t) \cdot Z_{\mathrm{IGBT}}(t)}{Z_{\mathrm{FWD}}(t) + Z_{\mathrm{IGBT}}(t)} \tag{4}$$

$Z_{\mathrm{arm}}(t)$ is the parallel thermal impedance of IGBT and FWD.

An IGBT module consists of two arms. The equivalent thermal impedance of the IGBT module could be expressed as:

$$Z_{\mathrm{mo}}(t) = \frac{Z_{\mathrm{arm}}(t)}{2} \tag{5}$$

$Z_{\mathrm{mo}}(t)$ is the equivalent thermal impedance of IGBT module chip.

Three IGBT modules in a three-phase two-level system generate the same heat in operation, the thermal impedance of the system $Z_{\mathrm{inv}}(t)$ could be expressed as:

$$Z_{\mathrm{inv}}(t) = \frac{Z_{\mathrm{mo}}(t)}{3} \tag{6}$$

In order to reduce the thermal resistance of the IGBT module copper substrate and radiator, the outer surface of the IGBT module copper substrate is generally connected to the radiator through the thermal grease. Therefore, the thermal resistance from the copper substrate to the radiator should include the interface thermal resistance of the three IGBT modules and the thermal resistance of the radiator body.

$$R_{\mathrm{ch}} = 3R_{\mathrm{gre}} + R_{\mathrm{int}}, \tag{7}$$

where R_{gre} is the interface thermal resistance of a single IGBT module; R_{int} is the thermal resistance of the radiator body.

The thickness, area and coefficient of thermal conductivity of thermal resistance R_{gre} coatings are correlated. Given the type of thermal conductive silicone grease, combined with the thickness d and area s of the coatings, the thermal resistance R_{gre} could be obtained by the following formula.

$$R_{\mathrm{gre}} = \frac{d}{\lambda \cdot s}, \tag{8}$$

where λ is the thermal conductivity of the thermal conductive silicone grease.

According to Fourier's basic law of heat conduction, the heat transferred through the unit cross-section area in unit time is proportional to the temperature change rate perpendicular to the cross-section direction, and the thermal resistance R_{int} of the radiator body could be calculated as [25]:

$$R_{\mathrm{int}} = \frac{l}{1.16 k_s L b n}, \tag{9}$$

where k_s is the thermal conductivity of the radiator, which is 175.6 kcal/h.m. at 20°C; L is the length of the radiator; l is the fin height of the radiator; b is the fin width of the radiator; n is the number of fins of the radiator.

In the process of air cooling and heat dissipation, the motor controller is placed in the engine cabin of the back end of the propeller. Air is disturbed by the front-end propeller, which causes the air flow in the radiator of the motor controller to be in "turbulent state". Assuming that the motor controller radiator is in a stable "turbulent state" during the flight of the aircraft, the heat transfer heat resistance R_{thk} between the radiator and the air could be expressed by the following formula [26].

$$R_{\mathrm{thk}} = \frac{\delta(T_{\mathrm{air}})^{-1/5} P_r(T_{\mathrm{air}})^{2/3}}{0.037 L^{4/5} b \cdot n \cdot \rho(T_{\mathrm{air}}) \cdot c_p(T_{\mathrm{air}}) \cdot v_s(t)^{4/5}}, \tag{10}$$

where $\rho(T_{\mathrm{air}})$ is the air density in kg/m^3; $c_p(T_{\mathrm{air}})$ is the specific heat capacity in J/kg.K; $v_s(t)$ is the air inlet speed of the radiator, the unit is m/s; $P_{\mathrm{r}}(T_{\mathrm{air}})$ is the Prandtl number; $\delta(T_{\mathrm{air}})$ is the dynamic viscosity coefficient, which is 1×10^{-5}m^2/s; T_{air} is the radiator working environment temperature and the unit is centigrade,which is considered to be 20°C during the test. The temperature rise in the engine compartment can be ignored due to the short duration of the aircraft during take-off phase.

The air density, specific heat capacity, Prandtl number and viscous coefficient could be fitted according to the air physical property table. The functional relationship of the working environment temperature of the radiator is shown in Eqn. (11).

$$\begin{cases} \rho(T_{\mathrm{air}}) = -2.02 \times 10^{-9} \times T_{\mathrm{air}}^3 + 4.663 \times 10^{-6} \\ \qquad \times T_{\mathrm{air}}^2 - 0.0036 \times T_{\mathrm{air}} + 1.298 \\ c_p(T_{\mathrm{air}}) = -3.6 \times 10^{-8} \times T_{\mathrm{air}}^3 + 6.26 \times 10^{-5} \\ \qquad \times T_{\mathrm{air}}^2 + 0.1022 \times T_{\mathrm{air}} + 1012 \\ \delta(T_{\mathrm{air}}) = -1.508 \times 10^{-9} \times T_{\mathrm{air}}^3 + 8.7 \times 10^{-6} \\ \qquad \times T_{\mathrm{air}}^2 + 0.009 \times T_{\mathrm{air}} + 1.32 \\ P_r(T_{\mathrm{air}}) = -2.588 \times 10^{-10} \times T_{\mathrm{air}}^3 + 5.247 \times 10^{-7} \\ \qquad \times T_{\mathrm{air}}^2 - 0.00025 \times T_{\mathrm{air}} + 0.71 \end{cases} \tag{11}$$

The thermal resistance of motor controller $Z_{\mathrm{co}}(t)$ can be expressed by Eqn. (3) ~ Eqn.(11):

$$Z_{\mathrm{co}}(t) = Z_{\mathrm{inv}}(t) + R_{\mathrm{ch}} + R_{\mathrm{thk}} \tag{12}$$

According to the basic definition of thermal impedance, the average junction temperature of IGBT module in motor controller $T_{\mathrm{vj}}(t)$ can be expressed as:

$$T_{\mathrm{vj}}(t) = T_{\mathrm{air}}(t) + Z_{\mathrm{co}}(t) P_m(t) \tag{13}$$

The temperature sensor in the IGBT module is placed in the silica gel near the IGBT chip, the actual temperature value collected in the IGBT module is consequently5 $\sim$ 8°C lower than that of the IGBT chip, the actual average temperature of IGBT module $T_{co}(t)$ can be expressed as [27]:

$$T_{co}(t) = T_{vj}(t) - 8 \tag{14}$$

According to the theory of material mechanics and fluid mechanics, fan speed and flow can be expressed by the following equation [28]:

$$\frac{M_{fan} \cdot n_{fan}(t)}{159.2} = \frac{F_{fan} \cdot Q_{fan}(t) \cdot \rho(T_{air}) \cdot g}{\eta_{fan}}, \tag{15}$$

where M_{fan} is the fan shaft torque; $n_{fan}(t)$ is the rotation speed of fan; F_{fan} is the average stress of fan blade; $Q_{fan}(t)$ is the fan flow rate, η_{fan} is the efficiency of fan; g is the acceleration of weight.

The fan shaft torque M_{fan} can be expressed as:

$$M_{fan} = 2\rho(T_{air}) \cdot g \cdot F_{fan} \cdot S_{fan} \cdot r_{fan}, \tag{16}$$

where S_{fan} is the effective stress area of fan blade; r_{fan} is the average stress radius.

The fan flow rate $Q_{fan}(t)$ can be obtained from Eqn. (15) and Eqn. (16):

$$Q_{fan}(t) = \frac{n_{fan}(t) r_{fan} \eta_{fan} S_{fan}}{79.6} \tag{17}$$

It can be seen from Eqn. (17) that for a given fan model, the effective force area, efficiency and force radius of the fan blade are approximately constant, so the relationship between fan speed and flow is approximately linear.

The wind velocity generated by fan can be approximated as [29]:

$$v_{fan}(t) = \frac{Q_{fan}(t)}{3600l \cdot d_r}, \tag{18}$$

where $v_{fan}(t)$ is the wind velocity generated by fan, which is the same as the air inlet speed of the radiator $v_s(t)$; d_r is the width of radiator.

Assuming that the aircraft is accelerating uniformly during the take-off phase, the inflow velocity is the same as the horizontal velocity during the take-off phase.

$$v_f(t) = v_{st} + \frac{v_c^2 - v_{st}^2}{2D_d} t, \tag{19}$$

where $v_f(t)$ is the horizontal velocity; v_{st} is the horizontal component of take-off speed; v_c is the cruising speed; D_d is the horizontal distance between the aircraft take-off and cruising.

The air inlet of the radiator of the motor controller is the same as the flight direction of the aircraft, air flow is affected by the wind resistance in the radiator, and speed of the radiator air inlet of the motor controller in the climbing stage of the aircraft can be approximated as:

$$v_{in}(t) = k_1 \frac{v_f(t)}{\cos\alpha}, \tag{20}$$

FIGURE 4. Two-seat manned electric aircraft.

where $v_{in}(t)$ is the air inlet speed of motor controller radiator during the take-off phase, which is the same as the fan wind speed $v_{fan}(t)$; α is the angle of climb, which is about 5°; k_1 is the loss factor of wind speed.

It can be obtained from Eqn. (15) $\sim$ Eqn. (20) that:

$$n_{fan}(t) = \frac{1.4k_1 l_m d_r (2D_d v_{st} + (v_c^2 - v_{st}^2)t)}{r_{fan}\eta_{fan}S_{fan}D_d \cos\alpha} \times 10^5 \tag{21}$$

Taking the fin height l_m of radiator of motor controller as optimization variable and other structural design parameters of radiator as constant, the objective function for optimizing the structure of air-cooled radiator is established as follows:

$$\begin{cases} T_{comax} = \max[f_1(V_{DC}(t), I_{DC}(t), U_{rms}(t), \\ \qquad I_{rms}(t), \cos\phi(t), n_{fan}(t), l_m)] \\ l_m = l - m\Delta l, \ m = 0, 1, 2 \cdots \dfrac{l}{\Delta l} \\ T_{co\,max} \le T_{max}, \end{cases} \tag{22}$$

where T_{max} is the maximum allowable temperature of the IGBT module; l_m is the given fin height of the air-cooled radiator; T_{comax} is the maximum temperature of IGBT module under the given fin height of radiator in the aircraft take-off phase; l is the fin height of radiator designed according to the rated power dissipation requirement of the motor controller; Δl is the step size.

When T_{max} is known, the optimization flow of the radiator structure of the motor controller is as follows:

(1) Given a step size Δl, let $n = 0$;
(2) Bring $l_1 = l$ into Eqn. (22) to calculate $T_{comax}^{[0]}$;
(3) Determine whether $T_{comax}^{[0]} - T_{max} \le 0.01$;
(4) If $T_{comax}^{[0]} - T_{max} \le 0.01$, then $l_1 = l$ is the optimal fin height of the air-cooled radiator;
(5) If $T_{comax}^{[0]} - T_{max} > 0.01$, let $n = 1$;
(6) Repeat steps (2), (3) until $T_{comax}^{[m]} - T_{max} \le 0.01$, the iteration ends;
(7) $l_m = l - m\Delta l$ is the optimum fin height of the air-cooled radiator, and $l/\Delta l > m \ge 1$.

IV. RADIATOR DESIGN OPTIMIZATION

In order to verify the effectiveness of the above optimization method, a two-seat manned electric aircraft, as shown in Fig. 4, is used to verify the motor controller radiator optimization method. Fig. 5 shows the IGBT module temperature variation characteristic curve of the motor controller during

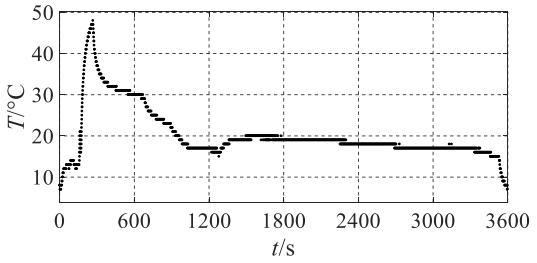

FIGURE 5. Characteristic curve of motor controller temperature.

FIGURE 6. The controller for two-seat electric aircraft.

TABLE 1. Motor controller design parameters.

Symbol	Quantity	Value
/	rated power	50kW
$V_{DC}(t)$	operating voltage	<=400VDC
/	effectiveness	95%
T_{max}	Maximum IGBT module work temperature(℃)	85℃

the completion of a flight. It can be seen from the characteristic curve that the IGBT module reaches its maximum junction temperature during the take-off phase of the aircraft, so this paper only analyzes the take-off phase of the aircraft. It can be assumed that the aircraft has a ground speed of 100km/h during the take-off phase, which generally last 90s, 120km/h during the cruise phase. The inlet wind speed of the motor controller radiator during the take-off could then be approximated. 50kW air-cooled motor controller, as shown in Fig. 6, is used for the taking-off phase. The radiator of the motor controller adopts a conventional fin-type structure, and the IGBT module in the motor controller is produced by Infineon. Three-phase two-level control system is used on a third-generation FF600R06ME3 module. The input DC voltage, DC current, output three-phase voltage, three-phase current and power factor of the motor controller are respectively collected through the power analyzer.

The design parameters of the motor controller, as shown in Table 1, need to meet the performance requirements of the aircraft.

In order to meet the heat dissipation requirements of the motor controller under actual operating conditions, the design parameters of the air-cooled radiator for motor controller

TABLE 2. The design parameters of radiator structure of air-cooled.

Symbol	Quantity	Value
/	material	aluminum
L	length	230mm
b	width	240mm
/	height	110mm
l	fin height	90mm
d_r	thickness	5mm
s	effective heat exchange area	1.05m^2
n	number of fins	30
/	weight	8kg

TABLE 3. Fourth-order foster model coefficient.

Order	R_i	R_j	τ
1	0.0054	0.009	0.01
2	0.0297	0.0495	0.02
3	0.0288	0.048	0.05
4	0.0261	0.0435	0.1

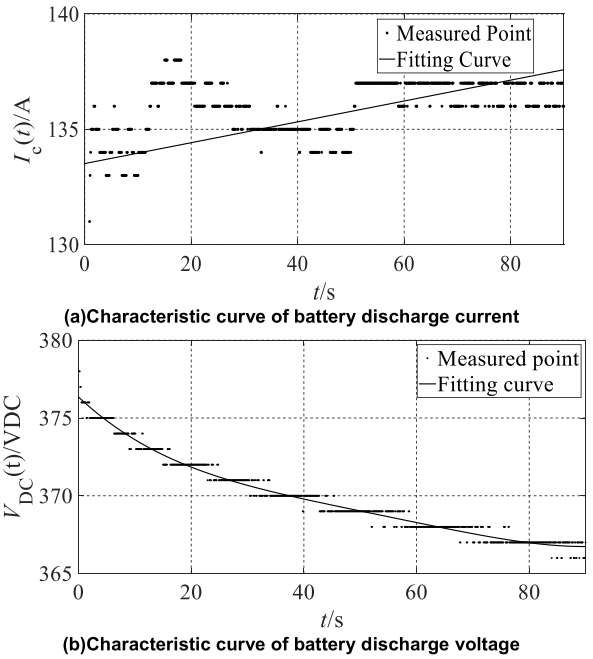

FIGURE 7. Characteristics curve of battery discharge current and voltage during take-off phase.

designed according to the rated power of the motor controller of 50kW are calculated and shown in Table 2.

The fourth-order foster model coefficients of IGBT and FWD can be obtained through the IGBT Module (FF600R06ME3) Manual, as shown in Table 3 [30].

The discharge characteristic curve of the battery during the actual take-off of a certain type of aircraft is shown in Fig. 7; the battery discharge voltage and current fitting coefficients obtained by fitting the actual battery discharge characteristic curve are shown in Table 4. The output current, voltage and power factor characteristics of the motor controller obtained

TABLE 4. Battery discharge voltage and current fitting coefficient.

Order	a_i	b_i
0	376.3	133.5
1	0.3377	4.519×10^{-2}
2	7.245×10^{-3}	0
3	8.889×10^{-5}	0
4	4.101×10^{-7}	0

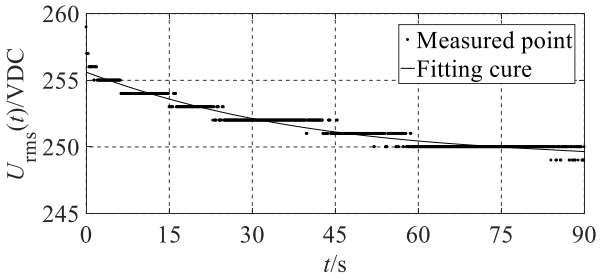

(a) Characteristic curve of output voltage

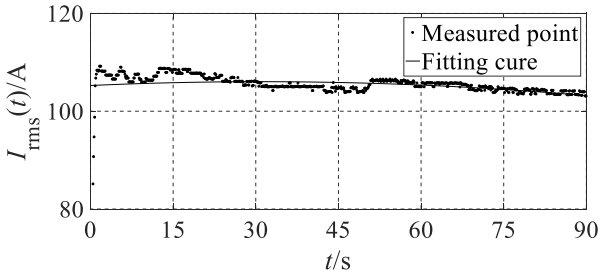

(b) Characteristic curve of output current

FIGURE 8. Characteristics curve of output voltage and current during take-off phase.

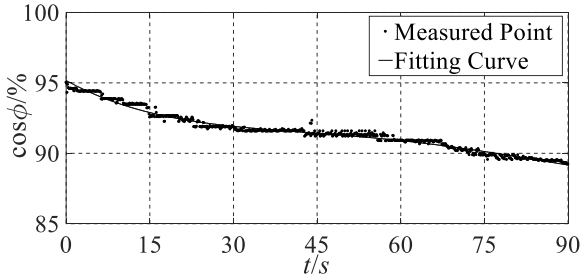

FIGURE 9. Characteristics curve of power factor during take-off phase.

TABLE 5. Output voltage, output current and power factor fitting coefficient.

Order	c_i	d_i	e_i
0	255.6	105.3	95.17
1	-0.156	0.05	-0.217
2	1.5×10^{-3}	8.17×10^{-4}	5.26×10^{-3}
3	-5.58×10^{-6}	0	-6.14×10^{-5}
4	0	0	2.4×10^{-7}

from the actual aircraft flight are shown in Fig. 8 and Fig. 9; the output voltage, current and power factor coefficients obtained by fitting the output characteristic curve of the motor controller are shown in Table 5.

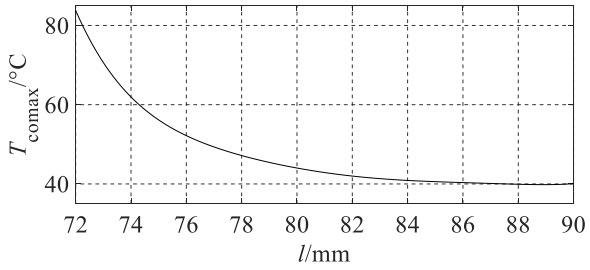

FIGURE 10. Temperature characteristic curve of IGBT module in take-off phase.

TABLE 6. Simulated flight profile of aircraft.

phase	Time(s)	Rotational speed of propeller (rpm)	Minimum power requirement(kW)
take-off	90	2450	45
cruise	3600	1650	14

TABLE 7. Performance parameters of fan.

Symbol	Quantity	Value
$n_{fan}(t)$	rotation speed range	0 ~ 6800rpm/min
r_{fan}	average stress radius	30mm
η_{fan}	efficiency	90%
S_{fan}	effective stress area of fan blade	$706mm^2$
/	power	3W

Assuming that the ambient temperature is 20°C, the characteristic curve of radiator fin height and IGBT module temperature change calculated according to the above optimization method of radiator fin height is shown in Fig. 10.

When the fin height of the air-cooled controller reaches 72mm during the take-off phase, the temperature of the IGBT module reaches 84.5°C, which is close to the allowable temperature of the IGBT module. Therefore, the fin height of the 72mm controller air-cooled radiator is the minimum allowable height.

V. PROTOTYPE TEST

A ground test was carried out using the test prototype as shown in Fig. 4.Two air-cooled radiator motor controllers with fin heights of 90mm and 72mm are respectively installed on the test prototype for testing. The simulated flight profile is shown in Table 6, a 612NHH-118 type fan is selected to simulate wind speed, and the performance parameters of the fan are shown in Table 7.The temperature of the motor controller IGBT module is recorded at every 0.1s during the 90s take-off interval.

The flight operation profile contains two main phases, take-off phase and cruise phase. Fig. 11 and Fig. 12 shows the temperature characteristic curve of IGBT module when the motor controller with radiator fin height of 90mm and 72mm reaches stable temperature rise, respectively.

The IGBT module temperature characteristic curve when the radiator fin height of 90mm is shown in Fig. 11. The

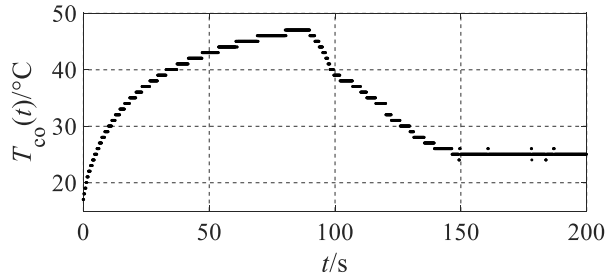

FIGURE 11. Characteristic curve of controller temperature when reaching steady state (90mm fin height).

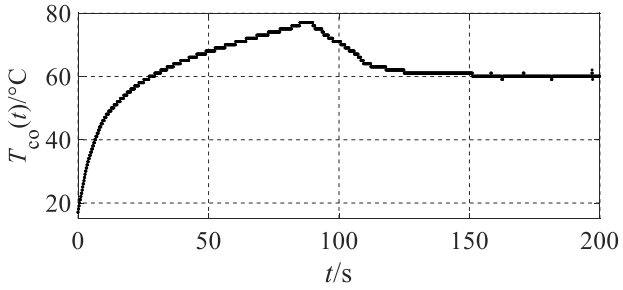

FIGURE 12. Characteristic curve of controller temperature when reaching steady state (72mm fin height).

temperature of the IGBT module during the simulation flight phase is up to 47 °C during the whole test. Fig. 12 shows the temperature characteristic curve of the IGBT module when the height of the radiator fin is 72 mm, while the temperature of the IGBT module during the flight phase is 77 °C during the whole test, which does not exceed the allowable temperature of the IGBT module in the motor controller manual(85 °C). The result of the prototype test is lower than the simulation result. The reason for this error is that the thermistor in the IGBT module is placed in the silica gel near the IGBT chip, and the heat insulation effect of the silica gel causes the measured temperature to be lower. Therefore, the effectiveness of the optimization method is demonstrated from the results of the prototype test. The 72mm wing high air-cooled radiator can meet the heat dissipation requirements of the electric aircraft motor controller, and the weight is reduced by 5% compared with the 90mm wing high air-cooled radiator. The heat dissipation structure of electric aircraft air-cooled controller is optimized.

Actual flight characteristics and ground simulated flight test characteristics when the height of radiator fins 90mm are shown in Fig. 5 and Fig. 11. It can be seen from the characteristic curve that the heat dissipation efficiency of the motor controller of the variable speed fan used to simulate the actual flight is slightly lower than that of the aircraft in the actual flight. Therefore, the radiator size designed according to the ground simulation flight test can satisfythe actual flight cooling requirements of the line process.

VI. CONCLUSION

This paper proposes a novel optimized design flow for air-cooled radiator based on studying the heat dissipation structure of the electric aircraft motor controller radiator. Unlike conventional design methods which rely on rated power consumption, the proposed method can reduce the weight and the size of the radiator while ensuring the flight safety of the aircraftby optimizing the heat dissipation structure of the electric motor controller based on the actual operating conditions of the electric aircraft. The proposed method focuses on the temperature of the IGBT module, which can simplify the analysis complexity while maintain a relatively accurate analysis of heat dissipation. Experimental results obtained from a prototype test on a two-seat electric aircraft shows that performance parameters calculated using the proposed method are very close to the results collected, which provides a theoretical basis for the optimization of controller radiator design. The proposed method can reduce weight of the radiator by 5% compared to the one designed using conventional method, which suggest the effectiveness of the proposed method. This work suggests a new approach in electric aircraft controller radiator design. We believe that it could be further extended and improved by taking additional parameters into consideration, such as shape and thickness of radiator fin, engine cabin temperature and external environmental parameters.

REFERENCES

[1] J. Huang and F. Yang, "Development and challenges of electric aircraft with new energies," *Acta Aeronautica et Astronautica Sinica*, vol. 37, no. 1, pp. 57–68, 2016.

[2] J. P. Bazzo, T. Lukasievicz, M. Vogt, M. L. S. Martins, H. J. Kalinowski, and J. C. C. Silva, "Performance evaluation of an IGBT module by thermal analysis using fiber Bragg grating," *Proc. SPIE*, vol. 7653, Sep. 2010, Art. no. 76533Y.

[3] C. Jiang, Z. G. Tang, H. Q. Li, and J. X. Hao, "Design of air-cooled radiator for IGBT controller of motor controller," *J. Automot. Eng.*, vol. 5, no. 3, pp. 186–1789, 2015.

[4] S. Dai and Y. Li, "Applied research of the intelligent temperature-controlled speed adjustable motor in radiator fan," in *Proc. ISDEA*, Jan. 2012, pp. 779–782.

[5] S. Ma, S. Wang, C. Zhang, and S. Zhang, "A method to improve the efficiency of an electric aircraft propulsion system," *Energy*, vol. 140, pp. 436–443, Dec. 2017.

[6] S. L. Wang, S. H. Ma, and S. Zhang, "Calculation and improvement for air cooling structure of electrical aircraft motor controller," *Electr. Mach. Control Appl.*, vol. 46, no. 6, pp. 1–7, 2019.

[7] G. W. Kang, Y. Hu, Y. D. Li, W. H. Jiang, "Research on parameters matching of ultralight electric aircraft propulsion system," *Hangkong Dong liXuebao/J. Aerosp. Power*, vol. 28, no. 12, pp. 2641–2646, Dec. 2013.

[8] L. Kong, Z. Dong, P. Ning, Z. Ji, and Q. Zhijie, "The IGBT module layout design considering the electrical and thermal performance," in *Proc. ITEC Asia–Pacific*, Aug./Sep. 2014, pp. 1–5.

[9] Z. K. Lu, "Thermal simulation and air cooling design of electric aircraft engine compartment," Ph.D. dissertation, Shenyang Aerosp. Univ., Shenyang, China, 2018.

[10] B. Xu, X. C. Li, and L. Peng, "CFD optimization of design for IGBT air-cooled heat sink," *Adv. Mater. Res.*, vols. 562–564, pp. 755–758, Apr. 2012.

[11] H. Kwon, W.-S. Lee, G.-T. Kim, and H. Park, "Numerical investigation on performance of air-cooled BLDC motor," *Trans. Korean Soc. Mech. Eng. B*, vol. 42, no. 10, pp. 681–687, Oct. 2018.

[12] Y. Li, J. Shang, S. Zhu, A. Ma, R. Lyle, Z. Li, N. Wang, and H. Rong, "Highly integrated and high efficiency motor controller based on double-sided cooling IGBT module," SAE Technical Papers 2017-01-2456, 2017.

[13] C. Jin, D. Wu, and Y. H. Shen, "Heat dissipation design and analysis of large power inverters for electric drive off-road mine truck," *Adv. Mater. Res.*, vol. 681, pp. 142–146, Apr. 2013.

[14] C. Qian, A. M. Gheitaghy, J. Fan, H. Tang, B. Sun, H. Ye, and G. Zhang, "Thermal management on IGBT power electronic devices and modules," *IEEE Access*, vol. 6, pp. 12868–12884, Jan. 2018.
[15] M. Chen, A. Hu, and X. Yang, "Predicting IGBT junction temperature with thermal network component model," in *Proc. Asia–Pacific Power Energy Eng. Conf.*, Mar. 2011, pp. 1–4.
[16] Z. K. Zhou, B. Liu, J. Li, Y. T. Wan, L. X. Du, and C. Wang, "Optimization design of heat Sink fins based on genetic algorithm," *Electro-Mech. Eng.*, vol. 35, no. 5, pp. 29–33, 2019.
[17] G. Romeo, F. Borello, and E. Cestino, "Design of inter-city transport aircraft powered by fuel cell & flight test of zero emission 2-seater aircraft powered by fuel cells," in *Proc. ESARS*, vol. 2012, Oct. 2012, pp. 1–7.
[18] K. X. Wei, C. N. Zhang, and Y. G. Dong, "Thermal coupling modeling for multi-chip paralleled igbt modules based on the thermal resistance network method," *J. Beijing Inst. Technol.*, vol. 26, pp. 147–152, Dec. 2017.
[19] S. Wang, S. Zhang, and S. Ma, "An energy efficiency optimization method for fixed pitch propeller electric aircraft propulsion systems," *IEEE Access*, vol. 7, pp. 159986–159993, Dec. 2019.
[20] Q. Kang, "Thermal simulation and thermal analysis of aircraft engine compartment," Ph.D. dissertation, Northwestern Polytech. Univ., Xi'an, China, Tech. Rep., 2007.
[21] D. Cavaiuolo, M. Gargiulo, A. Irace, and G. Breglio, "Design of an electric motor controller with embedded dynamic thermal control logic for motorbike racing application," in *Proc. IEVC*, vol. 2012, Mar. 2012, pp. 1–5.
[22] G. L. Lin, G. Q. Xu, W. M. Li, and B. B. Liu, "Thermal analysis of cold plate for motor controller based on fluent," *Appl. Mech. Mater.*, vols. 249–250, pp. 691–695, Dec. 2013.
[23] Y. F. Zhou *et al.*, "Design for motor controller in hybrid electric vehicle based on vector frequency conversion technology," *Automot. Elect. Appliances*, no. 7, pp. 1–6, Jul. 2010.
[24] Z. Pan, X. Jiang, H. Lu, L. Huang, S. Azuma, M. Kimata, and M. Seto, "Junction temperature analysis of IGBT devices," in *Proc. IPEMC*, vol. 3, Aug. 2000, pp. 1068–1073.
[25] J. Wu, L. Zhou, P. Sun, and X. Du, "Control of IGBT junction temperature in small-scale wind power converter," in *Proc. IEEE PEAC*, vol. 2014, Feb. 2014, pp. 41–48.
[26] Y. Yuan, D. Xiang, and C. Ning, "Self-calibration for IGBT junction temperature measurement in power converter," in *Proc. IEEE 8th Int. Power Electron. Motion Control Conf. (IPEMC-ECCE Asia)*, vol. 2016, May 2016, pp. 3125–3130.
[27] X. Xin, C. Zhang, and J. Zhao, "Electro-thermal based junction temperature estimation model and thermal performance analysis for IGBT module," in *Proc. 20th Int. Conf. Electr. Mach. Syst. (ICEMS)*, Aug. 2017, pp. 1–6.
[28] L. L. Song *et al.*, "Computational fluid dynamics analysis for flow field of radiator air intake in the powertrain compartment," *Appl. Mech. Mater.*, vol. 464, pp. 171–175, Nov. 2013.
[29] L. J. Li and H. J. Zhang, "Numerical analysis of heat transfer in the tree-like radiator with air cooling for a high power thyristor," *Amer. Soc. Mech. Eng., Heat Transf. Division*, vol. 237, pp. 111–115, Aug. 1993.
[30] (2013). *FF600R06ME3 Technical Information*. [Online]. Available: https://www.infineon.com/dgdl/Infineon-FF600R06ME3-DS-v03_01-en_cn.pdf?fileId=db3a30433e16edf9013e17138eba004c

SHULI WANG was born in Tangshan, China, in 1981. He received the master's degree in electric machines and electric apparatus from the School of Electrical Engineering, Shenyang University of Technology, in 2009, where he is currently pursuing the Ph.D. degree. He is also an Electrical Engineer with the Key Laboratory of General Aviation, Shenyang Aerospace University. His research interests include the modeling and optimal control of motor driving systems of electric aircraft.

XING CUI received the Ph.D. degree in vehicle engineering from the Beijing Institute of Technology, Beijing, China, in 2007.

He is currently a Senior Research Fellow with the North Vehicle Research Institute, China North Industries Group Corporation (NORINCO). His research interests include unmanned ground vehicle design, multimotor driving systems, distributing drive and control systems, and system integration.

SHAOHUA MA received the bachelor's and Ph.D. degrees in electrical engineering from the Shenyang University of Technology, in 1988 and 2008, respectively. She is currently a Professor with the School of Electrical Engineering, Shenyang University of Technology. She has been appointed as the Head of the Department of Electrical Machinery, since 2014. Her research interests include renewable energy generation, intelligent electrical apparatus, and advanced digital control technique and power electronics applications in power systems.

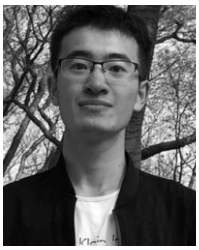

ZHEYUAN PANG received the bachelor's degree in electrical engineering from the Shenyang University of Technology, in 2018, where he is currently pursuing the master's degree. His research interest includes temperature rise model, including optimizing the heat dissipation structure by using an algorithm and switching power supply structure design.

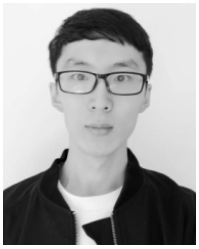

YUNING FENG received the bachelor's degree in automation from Dalian Polytechnic University, in 2016, and the master's degree in electrical engineering from the Shenyang University of Technology, in 2019, where he is currently pursuing the Ph.D. degree. His research interests include FEM and FVM algorithm in the field of electrical appliances, such as MHD and PIC model, including simulation of arc before and plasma.

SHUO ZHANG received the B.Eng. degree from the North China Institute of Aerospace Engineering, Hebei, China, in 2011, and the Ph.D. degree in vehicle engineering from the Beijing Institute of Technology, Beijing, China, in 2017.

He is currently an Assistant Professor with the National Engineering Laboratory for Electric Vehicles and the School of Mechanical Engineering, Beijing Institute of Technology. His research interests include the modeling and control for the permanent magnet synchronous motor, multimotor driving systems, and hybrid power systems.